DOI: 10.1002/anie.201108324

Photonic Crystals

# Fabrication of Robust Optical Fibers by Controlling Film Drainage of Colloids in Capillaries**

*Shin-Hyun Kim,* Hyerim Hwang, and Seung-Man Yang**

Optical fibers have enabled the development of fast telecommunication and imaging technologies.[1] Since the development of glass fibers, transmission losses have decreased significantly and optical fibers have become indispensable to everyday life, from telecommunications and networking to illumination tools and medical endoscopes. However, optical fibers based on total internal reflection (TIR) incur inevitable losses at highly bent regions, as occur in compact optical circuits, and at solid cores of fibers owing to absorption and scattering. Researchers have developed photonic crystal fibers that can overcome the shortcomings of TIR-based optical fibers.[2] The band-gap properties of photonic crystal fibers reduce losses and enable new optical applications, such as fiber lasers and nonlinear devices. Photonic crystal fibers are prepared using a stack-and-draw procedure with glass capillaries, or by drawing hollow tubes of concentric multilayers.[3]

Herein, we present a new type of photonic crystal fiber using a bottom-up approach involving spontaneous crystallization of colloidal particles. The self-organization of colloidal particles provides a practical approach to creating three-dimensional photonic crystals with potential utility in photonic circuits, laser cavities, or biosensors.[4] To fabricate colloidal crystal fibers, Moon et al. and Li et al. coated the outer surfaces of glass fibers with colloidal crystals using evaporation-induced vertical deposition.[5] However, extremely long fabrication times and poor mechanical properties have severely restricted the applications of these fibers, and the effects of the photonic band gap on light guiding have not yet been characterized. To create colloidal photonic crystal fibers in a practical and reproducible fashion, colloids were dispersed in a photocurable resin, resulting in spontaneous crystallization of the colloids with a repulsive potential; this resin is coated on the inner walls of microcapillaries under film-draining protrusion flow. Spontaneous crystallization and fast consolidation of the structures yielded robust photonic crystals with excellent optical performance. The controlled dynamic deposition of film on the microcapillaries permitted manipulation of the thickness and number of layers in the hollow photonic crystal fibers. Using photonic crystal fibers, we demonstrated that a stop band in a colloidal photonic crystal could enhance the efficiency of light guidance through the fibers away from the TIR regime.

This strategy relied essentially on film formation over the inner walls of the microcapillaries. To make a hollow fiber with a colloidal structure, a photocurable suspension of silica particles dispersed in ethoxylated trimethylolpropane triacrylate (ETPTA) was injected in the hydrophobic capillary. An aqueous surfactant solution was then forced through the capillary to drain the suspension out, maintaining a thin film of the suspension on the inner wall of the capillary owing to the hydrophobic nature of the surface (Figure 1a); surfactant solutions reduce interfacial energy between the solution and the suspension, enabling a stable formation of the film (Supporting Information, Figure S1). Upon application of UV irradiation, the film polymerized, producing a hollow cylindrical silica–ETPTA composite film on the inner wall of the capillary. During film formation, the small Reynolds number and small radius of the capillary produced insignificant gravitational and inertial forces so that the flow was governed by viscous and surface tension forces.[6] In the limit of a small capillary number ($Ca = \eta V/\gamma$), the surface tension forces dominated the viscous forces so that the relative thickness of the film $e/(b-e)$ was determined by the capillary number (Figure 1b), where $\eta$ is viscosity of the resin, $V$ is flow velocity of the aqueous solution, $\gamma$ is the interfacial energy, and $e$ and $b$ are the thickness of the film and the inner radius of the capillary, respectively. The dependence of the thickness on two parameters, $V$ and $\eta$, is illustrated in Figure S2 of the Supporting Information. The flow rate was controlled by a syringe pump, and the viscosity was modulated by adjusting the concentration of silica particles in the ETPTA resin. The relative thickness was proportional to $Ca^{2/3}$, in accordance with Bretherton's equation.[6b] Therefore, the relative thickness of the film could be controlled by the flow rate of an aqueous solution in the range 0.05–0.25. This coating method was effective, even for tubes longer than a few tens of centimeters (Supporting Information, Figure S3).

A coating formed from a highly concentrated silica–ETPTA suspension on a polyethylene (PE) tube produced structural colors that are due to the silica–ETPTA composite layer, which formed a narrow distribution of interparticle distances without long-range order.[7] Because the silica particles ($n_{silica} = 1.45$) dispersed in ETPTA ($n_{ETPTA} = 1.4689$) exhibit negligible van der Waals attractions owing to the small

[*] Dr. S.-H. Kim, H. Hwang, Prof. S.-M. Yang
National Creative Research Initiative Center for Integrated Optofluidic Systems and Department of Chemical and Biomolecular Engineering, KAIST
Daejeon, 305-701 (Korea)
E-mail: dmz@kaist.ac.kr
smyang@kaist.ac.kr
Homepage: http://msfl.kaist.ac.kr

[**] This work was supported by a grant from the Creative Research Initiative Program of the Ministry of Education, Science and Technology for "Complementary Hybridization of Optical and Fluidic Devices for Integrated Optofluidic Systems."

Supporting information for this article is available on the WWW under http://dx.doi.org/10.1002/anie.201108324.

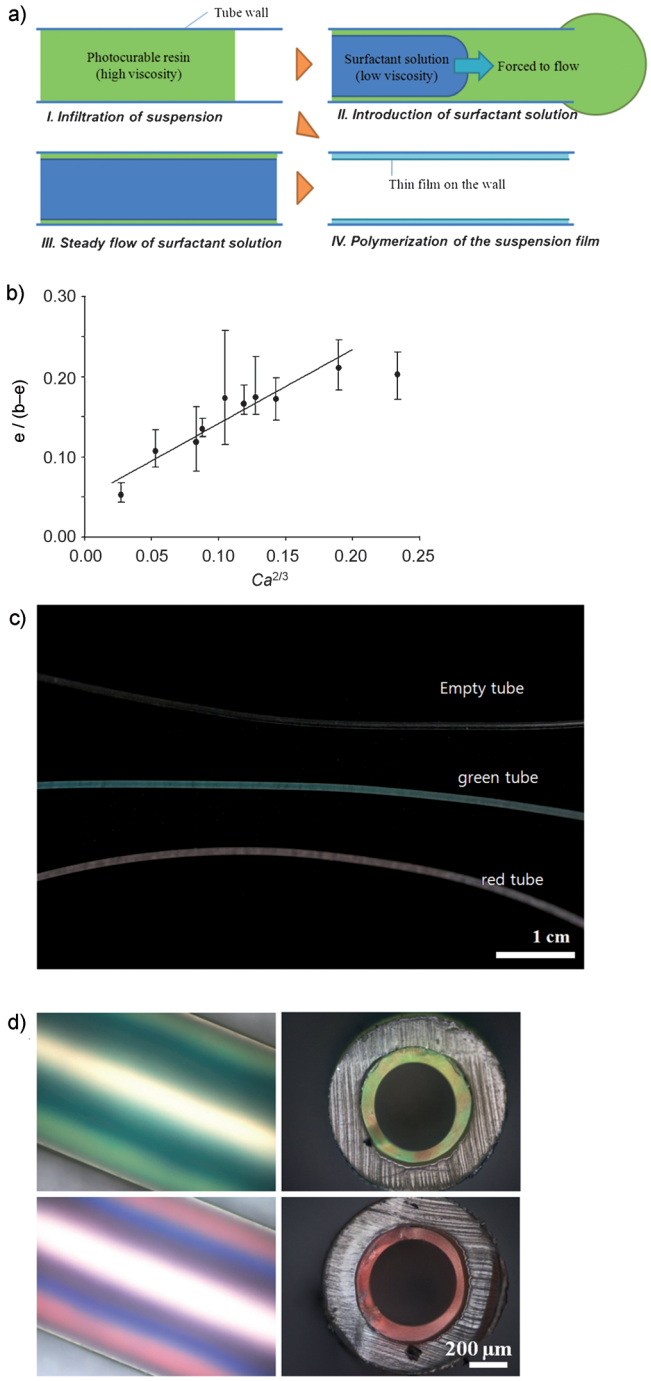


***Figure 1.*** a) Illustration of the coating procedure using the photocurable resin. b) The relative thickness as a function of the capillary number. c) Optical images of the tubes, the inner walls of which were coated with silica–ETPTA suspensions, resulting in green and red colors. For comparison, an uncoated tube is included. d) Optical microscopy (OM) images of the tubes with green- and red-colored layers.

index contrast, repulsive interparticle interactions dominate at short range because of the presence of a solvation layer on the silica particle surfaces.[8] Therefore, the particles maintain a distance with their neighbors without forming aggregates. As shown in Figure 1 c,d, the colorless PE tubes appeared green or red after coating with 168 nm or 190 nm silica particles in a volume fraction $\phi$ of 0.33, respectively. The colors were identical for both the cylindrical film surfaces and film cross-sections under normal incident light owing to the absence of long-range order.[9]

Multilayer films can be prepared by applying sequential suspension coatings. As shown in Figure 2 a, a cross-section of the bilayer, prepared in two coating steps, appeared green and red at the inner and outer layers, respectively. The reflectance spectra of the red and green single-colored layers and dual-colored bilayers are shown in Figure 2 b. Scanning electron microscopy (SEM) images of a vertical cut of the bilayer are shown in Figure 2 c,d. The boundary between two layers is apparent in these images, where the inner layer consists of 168 nm silica particles and the outer layer consists of 190 nm silica particles. The silica particles formed non-close-packed structures without long-range order. A multilayer consisting of red-, green-, and blue-colored composite layers is shown in Figure 2 e, prepared by applying sequential coatings in up to six steps. Furthermore, the outer diameter of the coating layer

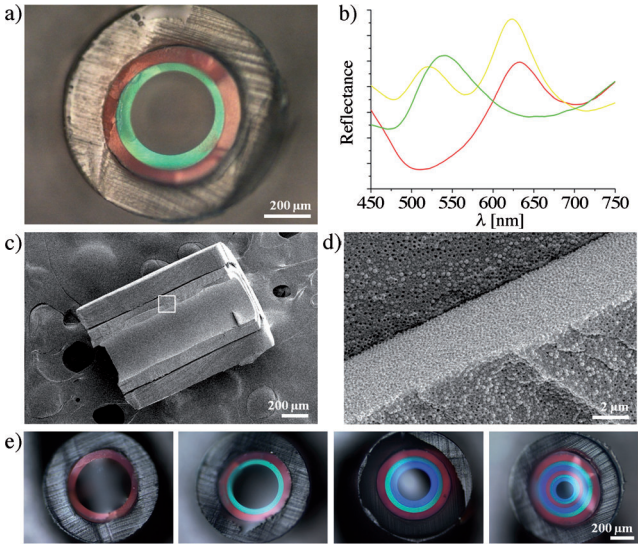


***Figure 2.*** a) OM image showing the cross-section of a tube coated with two distinct layers consisting of an inner green- and an outer red-colored layer. b) Reflectance spectra of the red-colored layer, green-colored layer, and dual-colored bilayer (shown as yellow). c,d) SEM images showing a vertical cut of the bilayer. The boundary between the two layers is shown in (d). e) Sequential coating of up to six layers using three different colored suspensions. Scale bars: 200 µm (2 µm in (d)).

can be controlled by inner diameter of templating tubes (Supporting Information, Figure S4).

The use of glass capillary tubes in place of PE tubes led to highly ordered structures. The inner walls of the glass capillary were treated with octadecyltrichlorosilane (OTS) to make the surfaces hydrophobic prior to introducing the suspension.[10] The glass capillary surfaces have a solvation layer even after OTS treatment, so that the walls and particles repel one another, initiating crystallization of the silica

  

particles on the wall upon application of a shearing force during injection. The crystals grew toward the center of the tube under repulsive interparticle interactions.[11] Although the composite coatings on the glass wall exhibited ordered structures, the reflective color was insignificantly enhanced from the composite coating on the wall of the PE tube (Figure 3a); this is attributed to the small refractive index contrast between the silica particles and the ETPTA, which induces a long attenuation length for Bragg's diffraction. To increase the contrast, silica particles were selectively etched away to produce a porous fiber with vivid reflection colors, as shown in Figure 3b; the templating glass tubes were also removed by etching.

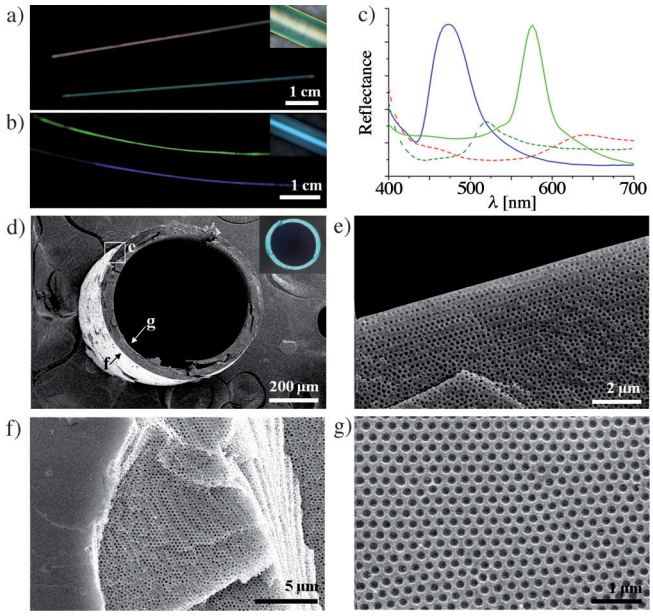


***Figure 3.*** a) Optical image of glass tubes coated with green- and red-colored composite layers. Inset: OM image of a tube coated with a green layer. b) Porous photonic crystal fibers colored green and violet. Inset: OM image of a violet-colored fiber, showing the blue reflected color of the normal reflection on the cylindrical surface. c) Reflectance spectra of the composite (-----) and porous (——) photonic crystal fibers shown in (a) and (b). d)–g) SEM images of a porous photonic fiber: cross-sections (d, e), a fractured outer surface (f), and an inner surface (g).

The reflectance spectra of the porous photonic fibers were blue-shifted relative to the peaks corresponding to the composite fibers owing to a decrease in the effective refractive index, and the reflection intensities were highly enhanced as a result of an increase in the refractive index contrast (Figure 3c). SEM images showing cross-sections of the porous photonic fibers are shown in Figure 3d,e, and the outer and inner surfaces are shown in Figure 3f,g, respectively. The repulsive forces between the glass wall and the silica particles produced smooth outer surfaces without pores, whereas the inner surfaces contained hexagonal arrays of dimples owing to the anchoring of the silica particles at the interface between the silica–ETPTA suspension and water.[12] The fractured region of the outer surface (Figure 3f) exhibits a hexagonal array of air pockets corresponding to the (111) plane of an fcc lattice. The arrays did not span a wide area because the fractured surface was not perfectly parallel to the cylinder surface. Alignment of the (111) plane along the cylindrical surface is attributed to nucleation of crystallization on the wall, which give rise to an L-gap all over the cylindrical surface.

We elucidated the effects of a photonic band gap on light confinement and guiding using porous photonic crystal fibers; cores of the fibers were infiltrated with particle-free ETPTA containing $10^{-4}$ M rhodamine B isocyanate and polymerized. The effective refractive index of the porous photonic crystal cladding ($n_{cladding} = 1.3325$ for $\phi = 0.33$) is smaller than that of the dye-doped solid core ($n_{core} = 1.4689$), which induces a critical angle for TIR of 65.11°. Therefore, incident beams with angles smaller than 65.11° experience significant losses. To investigate the band-gap-assisted guiding effects of the light in this off-TIR regime, we employed porous photonic crystal claddings with four different stop-band positions at 587 nm, 656 nm, 785 nm, or 855 nm, prepared using a suspension of silica particles 205 nm, 230 nm, 275 nm, or 300 nm in diameter at $\phi = 0.33$, respectively. Optical microscopy images and reflectance spectra of the four photonic crystal fibers are shown in Figure 4a,c. The first and second fibers had a stop band in the visible range, displaying brilliant reflection colors of green and red at the central position. The third and fourth fibers had stop bands in the infrared. The weak blue color on the fourth fiber resulted from second-order diffraction at 427.5 nm. The fiber with a stop band at 587 nm displayed one dark stripe parallel to the cylinder axis in the fluorescence microscopy image, as indicated by the arrow in the first image of Figure 4b. The photoluminescence (PL) spectrum of rhodamine B isocyanate in ETPTA core showed a peak at 602 nm, which spanned 580–700 nm. The emitted light with normal incidence on the surface, therefore, was reflected owing to the stop band at 587 nm, which produced a relatively dark central position in the fluorescence microscopy image. By contrast, the fiber with a stop band at 656 nm revealed a reflection maximum at 602 nm at an incident angle of 30° relative to the (111) plane, according to Bragg's law; this reflection gave rise to two parallel stripes along the left and right sides of the center, as indicated by the arrows in the second image of Figure 4b.

We measured the spectra at the ends of fibers 1.1 cm in length under normal excitation illumination to the surface of fiber with light of a mercury lamp at the other end (Figure 4d) to observe the effects of the photonic band gap on the guiding of emitted light. Figure 4e shows the changes in the reflectance maximum as a function of the incident angle plotted according to Bragg's law. The PL spectrum of rhodamine B isocyanate in ETPTA is plotted on the right-hand side and is shown as a red band in the intensity gradient of the main plot. The reflectance maximum for the fiber with a stop band at 587 nm overlapped with the PL spectrum only under normal incidence, as shown in the plot. The fiber with a stop band at 656 nm reflected emission at low angles, from 0° to 35°. However, the reflection at normal or low angles contributed insignificantly to light guiding owing to the large losses at multiple reflections (Figure 4e, illustration at lower left-hand

  

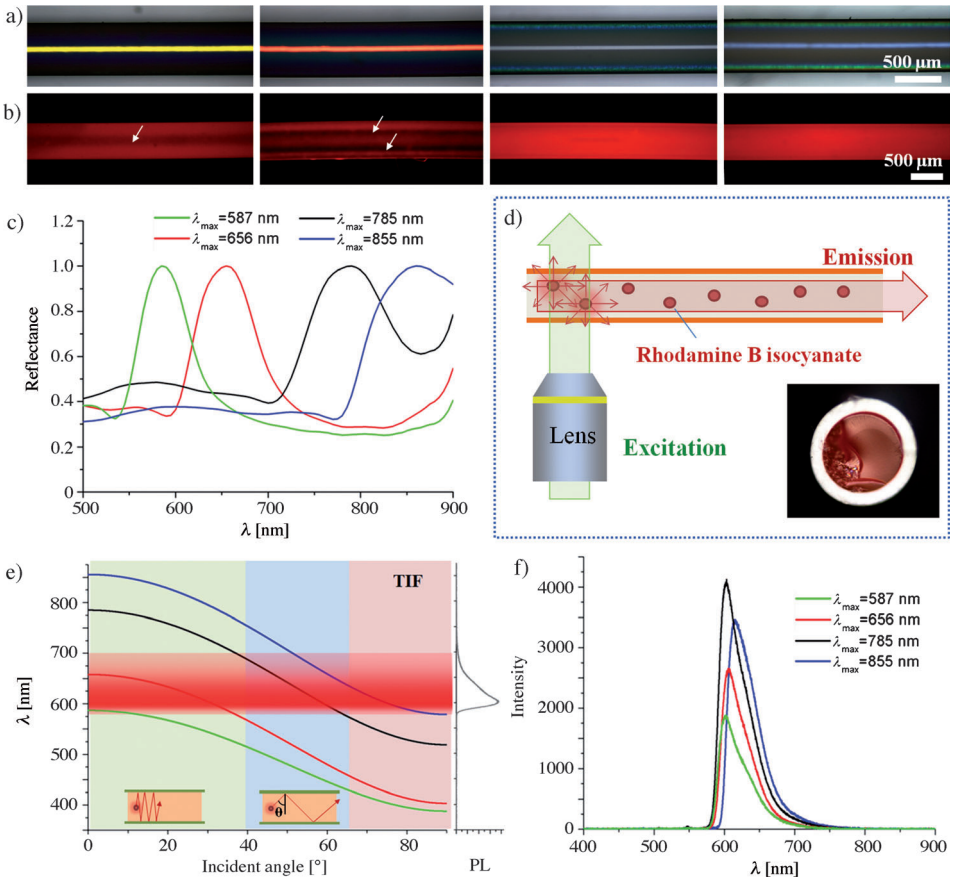


***Figure 4.*** a) OM images of four photonic crystal fibers, with different stop-band positions, that consist of a dye-doped core and a porous photonic crystal cladding. b) Fluorescence microscopy images of the four photonic crystal fibers shown in (a). c) Normalized reflectance spectra of the four photonic crystal fibers. d) Illustration of the photoluminescence (PL) measurement to evaluate the effects of the band gap on the guiding of light emitted from the dye molecules in the core. A cross-sectional image of a photonic crystal fiber is included to show a dye-doped solid core. e) Angular dependence of the Bragg's diffraction, showing the stop-band position optimal for guiding the emitted light, where the PL spectra of rhodamine B isocyanate is included on the right-hand side and is reproduced as a red band in the main plot. f) PL spectra measured at the ends of four photonic crystal fibers.

side). The reflectance maximum of the fiber with a stop band at 785 nm overlapped with the PL spectrum at relatively large angles, from 40° to 60°, which increased the guiding efficiency, as indicated by the blue background and illustrated in the corresponding cartoon. Figure 4 f shows the PL spectra measured at the ends of the four fibers. As expected, the fiber with a stop band at 785 nm yielded the highest intensity of guided light, with a peak at 602 nm. In contrast, the PL spectrum from the fiber with a stop band at 855 nm showed a peak at 615 nm, unlike the spectra from the three other fibers. Figure 4 e shows that the reflectance maximum of the fiber with a stop band at 855 nm overlapped with the PL spectrum between 630 nm and 700 nm at an incident angle of 55–65°. This overlap produced a red shift in the peak position of the PL spectrum collected at the end of the fiber.

In conclusion, photonic crystal fibers with hollow or solid cores were easily fabricated from spontaneous crystallization of colloids on the inner wall of microcapillaries. The dimensions of the fibers were also controlled by a capillary number and templating capillary during dynamic deposition of film. They may potentially provide alternatives to conventional optical or photonic crystal fibers. Furthermore, the colloidal photonic crystal fibers can be useful in specialized applications, including optical filters and resonators through additional development. Notably, curved fibers with small bending radii can be prepared using curved glass capillary templates (Supporting Information, Figure S5). This novel approach to coating the inner walls of tubes will also be useful for the creation of tailored nanoscale rough textures on microchannels for the study of nanofluidics or low-resistance pipes composed of superhydrophobic surfaces (Supporting Information, Figure S6).[13]

## *Experimental Section*

Monodisperse silica particles of various diameters were prepared using the Stöber method. An ethanol suspension of the silica particles was mixed with an ETPTA resin (Aldrich) containing 1 wt% photoinitiator (Irgacure2100, Ciba Specialty Chemicals). After complete mixing, the ethanol was selectively evaporated at 70 °C for 12 h. The volume fraction of silica particles in ETPTA in the ethanol-free base was carefully selected within the range 0–50 % (v/v) to make stop bands at the desired wavelength or to modulate the viscosity. The viscosity and interfacial tension were measured by rheometer (ARES, Rheometric Scientific) and tensiometer (Sigma 701, KSV), respectively.

The photocurable suspension was coated onto the inner walls of the tubes by introducing an aqueous solution of 1 wt% ethylene oxide–propylene oxide–ethylene oxide tri-block copolymer (Pluronic F108; BASF) into the tube containing the silica–ETPTA suspension. Two types of tube were employed: PE tubes with a 0.58 mm inner diameter (PE50; Becton Dickinson), and glass capillaries with a 0.58 mm inner diameter (1B100-3; World Precision Instruments, Inc.). The glass capillary tubes of various diameters were prepared by heating and pulling. The inner surfaces of the glass tubes were treated by incubation in a 6 mM OTS (Aldrich) solution in toluene at 70 °C for 30 min prior to infiltration of the suspension. The aqueous surfactant solution was introduced into the tube using a syringe pump (model 781200; KD Scientific) with a controlled flow rate, and the tubes coated with suspensions were irradiated with UV for one second to polymerize the film after reaching a steady-state flow. The glass capillaries coated with silica-ETPTA composite films were treated with a 5 % HF solution (Sigma–Aldrich) for 24 h to etch out the silica particles and glass capillary templates. A dye-doped core was prepared in the hollow porous photonic fiber by injecting a $10^{-4}$ M

ETPTA solution of rhodamine B isocyanate under capillary action, and the fibers were irradiated with UV for two seconds. The reflection spectra of the resultant photonic fibers were measured using an optical spectrometer (Ocean Optics, USB4000) equipped with an optical microscope (Nikon, L150). PL spectra and fluorescence images of the rhodamine B isocyanate-doped cores of the photonic crystal fibers were collected using a fiber-type optical spectrometer (Ocean Optics, USB4000) and a fluorescence microscope (Nikon, TE-2000U), respectively.

Received: November 25, 2011
Revised: January 23, 2012
Published online: March 1, 2012

**Keywords:** band gap · colloidal crystals · optical fibers · photonic crystals · photonic glass

[1] A. Ghatak, K. Thyagarajan, *An introduction to fiber optics*, Cambridge University Press, New York, **1998**.
[2] P. Russell, *Science* **2003**, *299*, 358.
[3] a) J. C. Knight, T. A. Birks, P. St. J. Russell, D. M. Atkin, *Opt. Lett.* **1996**, *21*, 1547; b) R. F. Cregan, B. J. Mangan, J. C. Knight, T. A. Birks, P. St. J. Russell, P. J. Roberts, D. C. Allan, *Science* **1999**, *285*, 1537; c) Y. Fink, J. N. Winn, S. Fan, C. Chen, J. Michel, J. D. Joannopoulos, E. L. Tomas, *Science* **1998**, *282*, 1679; d) K. Kuriki, O. Shapira, S. D. Hart, G. Benoit, Y. Kuriki, J. F. Viens, M. Bayindir, J. D. Joannopoulos, Y. Fink, *Opt. Express* **2004**, *12*, 1510.
[4] a) Y. Vlasov, X. Bo, J. Sturm, D. Norris, *Nature* **2001**, *414*, 289; b) Y. Xia, B. Gates, Z. Li, *Adv. Mater.* **2001**, *13*, 409; c) S. A. Rinne, F. Garcia-Santamaria, P. V. Braun, *Nat. Photonics* **2008**, *2*, 52.
[5] a) J.-H. Moon, G.-R. Yi, S.-M. Yang, *J. Colloid Interface Sci.* **2005**, *287*, 173; b) J. Li, P. R. Herman, C. E. Valdivia, V. Kitaev, G. A. Ozin, *Opt. Express* **2005**, *13*, 6454.
[6] a) G. Taylor, *J. Fluid Mech.* **1961**, *10*, 161; b) F. P. Bretherton, *J. Fluid Mech.* **1961**, *10*, 166.
[7] K. Ueno, A. Inaba, Y. Sano, M. Kondoh, M. Watanabe, *Chem. Commun.* **2009**, 3603.
[8] a) S. R. Raghavan, H. J. Walls, S. A. Khan, *Langmuir* **2000**, *16*, 7920; b) J. Ge, Y. Yin, *Adv. Mater.* **2008**, *20*, 3485.
[9] H. Noh, S. F. Liew, V. Saranathan, S. G. Mochrie, R. O. Prum, E. Dufresne, H. Cao, *Adv. Mater.* **2010**, *22*, 2871.
[10] S.-H. Kim, S.-H. Kim, S.-M. Yang, *Adv. Mater.* **2009**, *21*, 3771.
[11] a) S.-H. Kim, S.-H. Kim, W. C. Jeong, S.-M. Yang, *Chem. Mater.* **2009**, *21*, 4993; b) S.-H. Kim, W. C. Jeong, H. Hwang, S.-M. Yang, *Angew. Chem.* **2011**, *123*, 11853; *Angew. Chem. Int. Ed.* **2011**, *50*, 11649.
[12] a) B. P. Binks, S. O. Lumsdon, *Langmuir* **2000**, *16*, 8622; b) S.-H. Kim, S. Y. Lee, S.-M. Yang, *Angew. Chem.* **2010**, *122*, 2589; *Angew. Chem. Int. Ed.* **2010**, *49*, 2535.
[13] C.-H. Choi, C.-J. Kim, *Phys. Rev. Lett.* **2006**, *96*, 066001.

  